Chapter 4

Na^+ ion conducting polymer-NASICON hybrid composites

In the previous chapter, we discussed the electrical and structural properties of the Li^+ ion conducting polymer–NASICON composites. Such hybrids provide high ionic conductivity with appreciably enhanced Li^+ ion transference number. Due to the restricted availability of lithium, attention has also been on technology based on alternative ions [1][2][3]. Thus, in view of the need for developing new electrolytes based on other mobile ions, Na^+ ion based systems are the obvious choice due to the huge availability of sodium and similar insertion mechanism with that of Li^+ ions [4][5][6]. In this chapter, a thorough investigation on electrical and structural properties of novel Na^+ ion conducting solid polymer electrolyte, dispersed with two types of NASICONs (NTP & NZSP), is presented. The chapter explores the effect of NASICON concentration on electrical properties in a wide range of composition. It further assesses the role of electrical conductivity of NASICON in enhancing the overall total ionic conductivity of the polymer-NASICON hybrid. Also, it gives insights into the effect of salt concentration in enhancing the ionic conductivity particularly at higher concentrations of NASICON

(i) M.D. Singh, A. Dalvi, D.M. Phase, *Electricatransport in PEO-NaI-NASICON nanocomposites: An assessment using impedance and X-Ray absorption spectroscopy*, **Mater Res Bull. 118** (2019) 110485.
(ii) M. D. Singh, A. Dalvi, D M Phase, "*Novel $Na_5Zr_2Si_2PO_{12}$-polymer hybrid composites with high ionic conductivity for solid-state ionic devices*" **Materials Letters** 262 (2020) 127022.
(iii) M.D. Singh, A. Dalvi, S. Bharadwaj, A.M. Awasthi, "*Structural relaxation and electrical transport in NASICON reinforced Na^+ ion solid polymer electrolytes*" **AIP Conference Proceedings** 2265, 030611 (2020).

4.1 NaI-(PEO-NTP) system

To understand the effect of grain conductivity in the total conductivity of the polymer-NASICON composites, the current work discusses the dispersion of basic NASICON framework compound $NaTi_2(PO_4)_3$ (NTP).

In the current section, the compositions under discussion are $10NaI\text{-}90[PEO_{1-x}NTP_x]$ where $0 \leq x \leq 0.7$. Thus x = 0 will be abbreviated as 0 NTP, and similarly x = 0.1 as 10 NTP, and so on upto x = 0.7 as 70 NTP. Also, the samples with composition $x \leq 0.4$ were in film form, and for $x \geq 0.5$ in the pellet form.

4.1.1 X-ray Diffraction

Fig. 4.1 shows the XRD spectra for pure PEO, hybrid SPEs, and milled NTP sample. Crystallite size of NTP calculated using the Debye Scherrer formula was found to be ~ 30 nm. In case of film of pristine PEO two characteristics peaks are apparent at 18.3° and 22.6°. Further, when salt is added (0 NTP), area under the peaks corresponding to PEO get suppressed that may be due to considerable decrease in the PEO crystallinity. Interestingly when NTP is added to the matrix, the peaks corresponding to PEO are not only further suppressed, but also exhibit a notable shift that may be due to strain created at PEO-NTP interface.

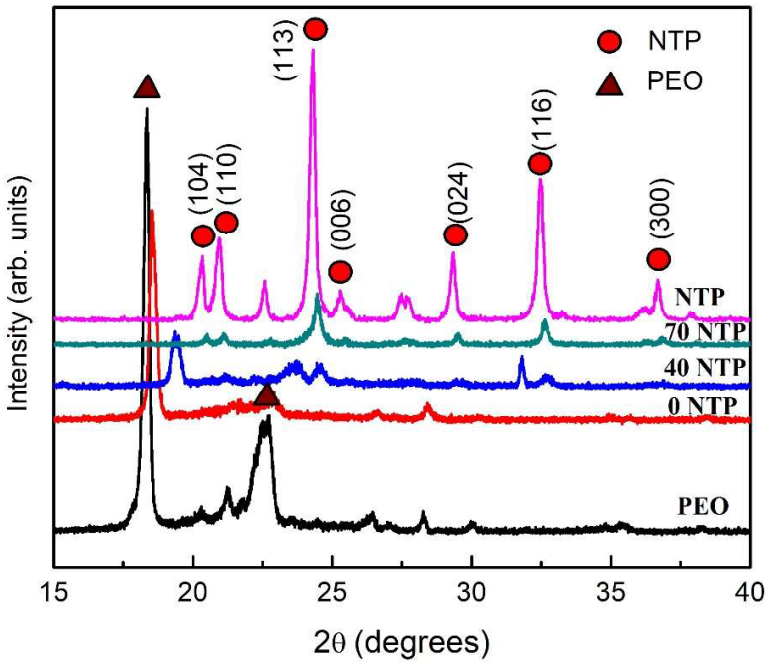

Figure 4.1 *XRD patterns for Pristine PEO film, composite SPEs (0 NTP, 40 NTP and 70 NTP) and milled NTP powder sample. Peak indexing as per* [7].

On further addition of NTP into the polymer matrix, for x = 0.7 (i.e. 70 NTP sample) the peaks corresponding to the PEO completely disappear, and those of NTP are predominantly seen with a subtle shift. Polymer crystallinity appears to be lost for the high content of NTP in the matrix. It is important to mention that the salt content is fixed to 10 wt% in the polymer matrix. However, O/Na ratio changes when NTP is added. Therefore, even for high NTP content where the O/Na ratio is low, salt remains in the dissolved state.

4.1.2 Elemental distribution

To understand the distribution of sodium and iodine (Na^+ and I^-) ions in the polymer matrix, EDS mapping was employed during FESEM characterization to confirm components and elemental distribution, particularly, for 40 NTP and 70 NTP hybrid composites. A combination of morphology along with elemental distribution is shown for 40 and 70 NTP samples in Fig. 4.2a and b, respectively.

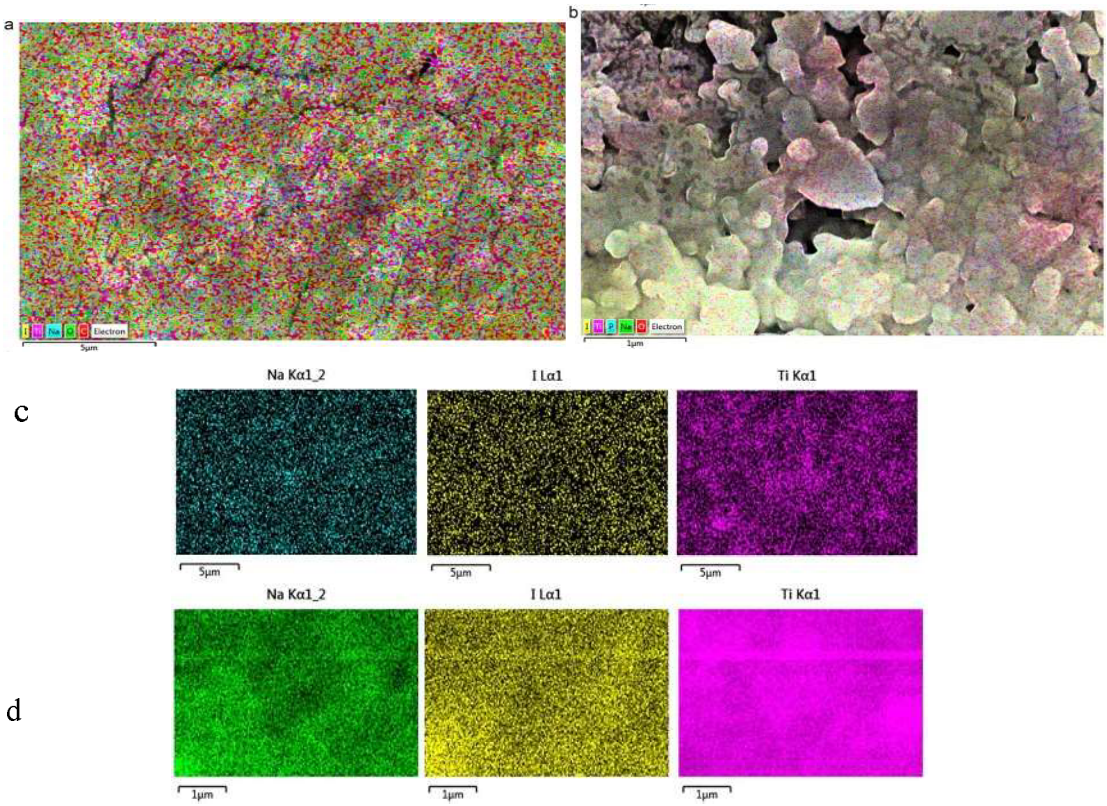

Figure 4.2 *EDS mapping over FE-SEM image for (a) 40 NTP and (b) 70 NTP hybrid composite. Total elemental distribution of Na, I, and Ti elements by EDS for (c) 40 NTP and (b) 70 NTP composite.*

For 40 and 70 NTP distribution of different elements, Na, I, and Ti appear dense as well as homogeneous. Total elemental mapping is also shown in Fig. 4.2c and d for 40 and 70 NTP samples. For 40 NTP, Titanium appears well distributed in the map, suggesting the homogeneous distribution of NTP nanoparticles in the matrix. As apparent, the salt ions appear uniformly distributed in both compositions. Additionally, the distribution of sodium appears denser (even on an extended scale) for 70 NTP.

4.1.3 Electrical properties

The frequency dependence of electrical transport is studied for 0-70 NTP samples. The conductivity exhibits a mostly similar trend when NTP is added but with certain notable changes, particularly for high NTP content. For two of the samples with moderate and high NTP content (viz. 40 NTP and 70 NTP), the σ-ω behavior is shown in Fig. 4.3a & b, respectively. For both the samples conductivity exhibits a plateau region followed by dispersion at higher frequencies. At lower frequency values, a significant fall is witnessed due to interfacial polarization that in turn also confirms a predominant ionic nature. In the inset of Fig. 4.3a, the Nyquist plot at 303 K is also shown where depressed semicircle followed by inclined line at low frequencies confirms typical ionic behavior of the composite.

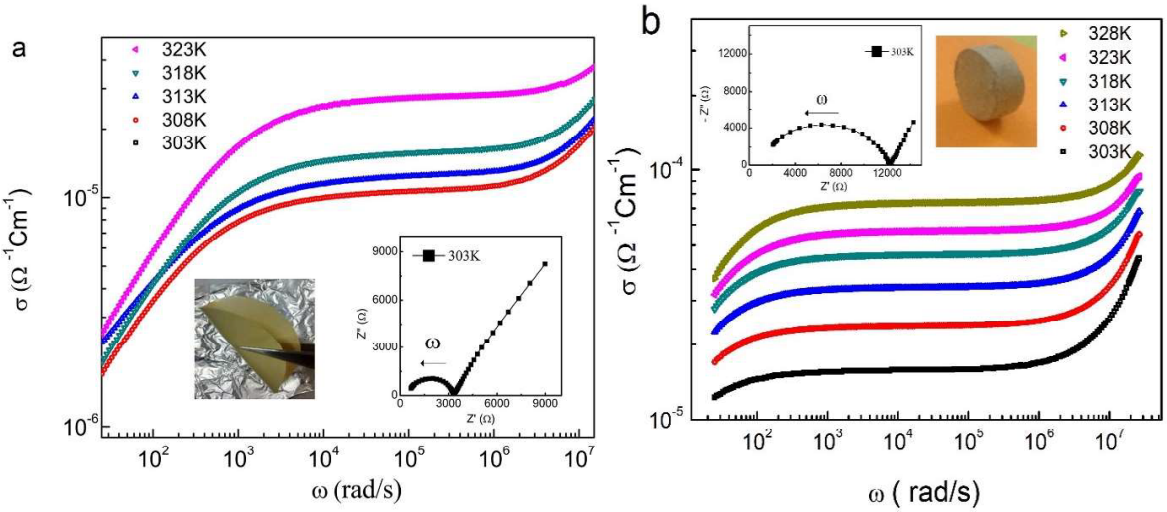

Figure 4.3 *(a) Frequency dependence of conductivity at various temperatures for 40 NTP hybrid composite. Inset: Nyquist plot at 303 K and photograph of film. (b) Frequency dependence of conductivity at various temperatures for 70 NTP hybrid composite. Inset: Nyquist plot at 303 K and photograph of pellet.*

In case of 70 NTP almost similar behavior is seen for σ-ω as well as Nyquist plot. Interestingly, the characteristics plateau region of dc bulk conductivity is appreciably wide in this case. An extended plateau region may also suggest relatively longer diffusion lengths for sample with higher NTP content. Therefore, an important role of embedded NASICON particles is expected in facilitating the bulk conduction process. From the Nyquist plot of 70 NTP, it may also be suggested that NTP crystallites do facilitate electrical transport. Secondly, no separate ingrain/grain boundary semicircles are visible that in turn suggest nominal grain boundary contribution to total electrical transport.

From the plateau of σ-ω plot, the bulk conductivity was obtained and plotted as a function of temperature in Fig. 4.4. Initially, the conductivity almost increases Arrheniusly for all samples. For the low NTP content samples, conductivity shows a notable deviation from linear behavior near the melting point of PEO. Interestingly, the deviation in conductivity shifts towards the higher temperature side with an increase in NTP content as also shown by the dotted line.

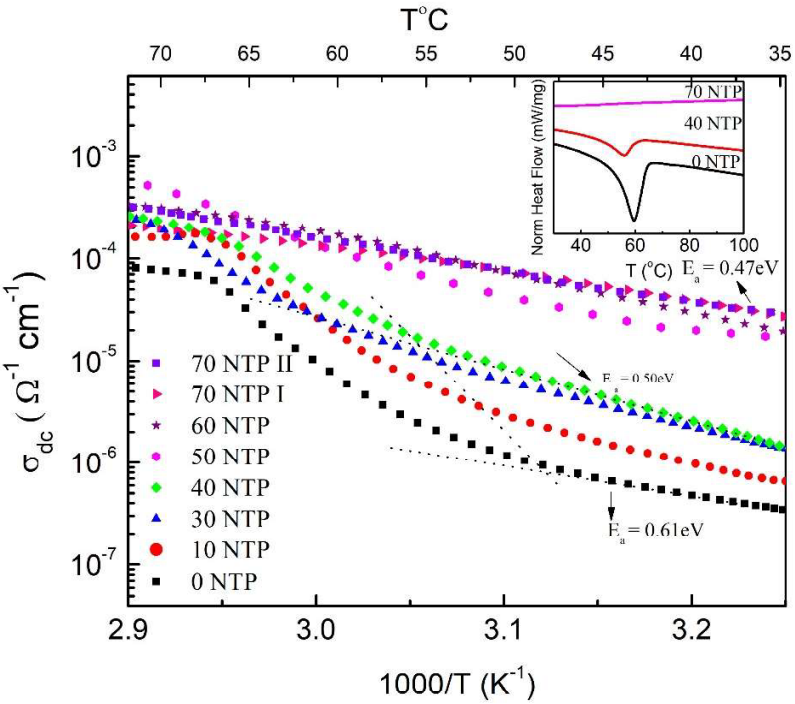

Figure 4.4 *Temperature-dependent dc conductivity for hybrid composites of composition 10NaI-90($PEO_{1-x}NTP_x$), $0 \leq x \leq 0.7$. Plot with 70 NTP I and 70 NTP II corresponds to first and second heating cycles for 70 NTP composite. Inset: DSC thermogram for 0, 40 and 70 NTP samples. The dashed line is a guide to the eye to show deviation from Arrhenius behaviour near melting of PEO.*

For high NTP content $x \geq 0.5$ interestingly, no such deviation at the melting point of the PEO is noticed. For these samples (pellet form) the cycles are truly reproducible at least up to 100 °C. Since polymer content notably reduces in these compositions due to NTP substitution, the melting event possibly leads to a less significant change in the conductivity. The same is also complemented by the DSC thermogram (inset) obtained by normalizing the heat flow with respect to PEO amount in composites, where the area under the melting dip of PEO gradually gets suppressed with NTP content and fully disappears for 70 NTP sample.

Further, scaling behavior for electrical conductivity with temperature for 70 NTP sample and with NTP content at 30 °C has been analyzed systematically. For scaling, dc conductivity is obtained from the plateau region and ω_{dc} is obtained from the fitting result of the Almond-west formalism as describe elsewhere [8].

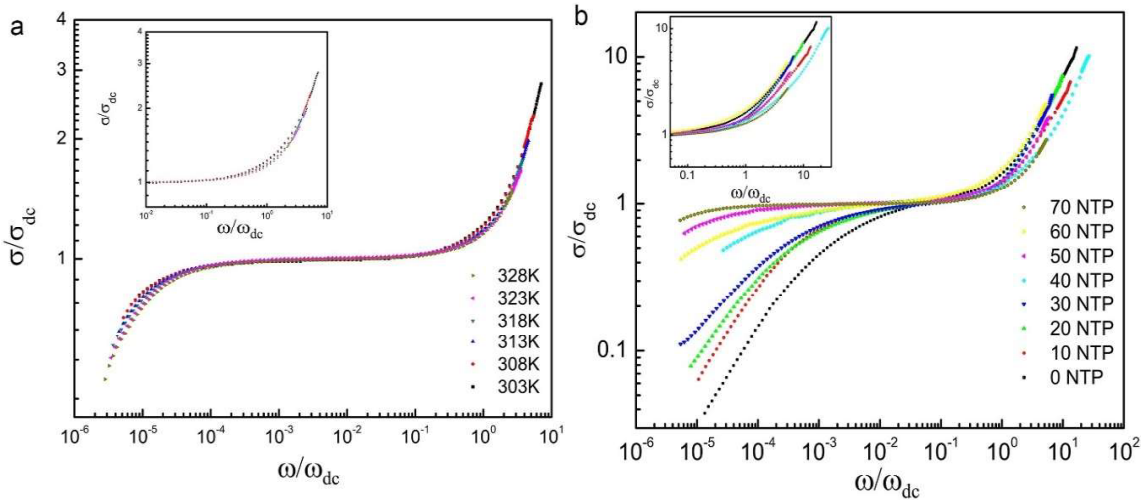

Figure 4.5 *(a) Conductivity scaling behaviour for 70 NTP composite with temperature variation. Inset: The same on an extended scale. (b) Conductivity scaling behaviour at room temperature with varied composition of NTP: 10NaI-90($PEO_{1-x}NTP_x$), $0 \leq x \leq 0.7$. Inset: The same on an extended scale.*

Fig. 4.5a represents the scaling behavior with temperature for 70 NTP sample, where the spectra at higher frequency region apparently superimposed into a single master curve. These suggest the same mechanism of ionic transport at different temperatures. Scaling behavior is however lost with NTP content as shown in Fig. 4.5b. There is an apparent deviation from the single master curve, more significantly noticed at lower frequencies. The inset of Fig. 4.5a and

b again shows the same on an extended scale. It may be readily suggested that the mechanism of electrical transport is very much influenced by NTP addition to the matrix.

Further, to understand the role of NASICON in electrical transport, low temperature conductivity behavior and structural relaxation was obtained. The ac conductivity and electric modulus were obtained in a frequency range of 10Hz-10MHz and studied as a function of temperature (220K -300K) with an interval of 4K.

The frequency dependence of ac conductivity for 0 NTP and 40 NTP samples is shown in Fig 4.6 (a) and (b). For 0 NTP the conductivity at low temperatures apparently exhibits two dc to dispersion regions (onset shown by arrows). At higher temperatures, high frequency plateau is though not distinguishable. The 40 NTP sample, however, exhibits only one apparent plateau spreading in a wide range of frequencies. The lower frequency plateau corresponds to long range diffusion of ions, and the one at higher frequency to structural relaxation of host polymer chains [9–12]. Thus the structural relaxation of host chains appears to be suppressed in 40 NTP sample.

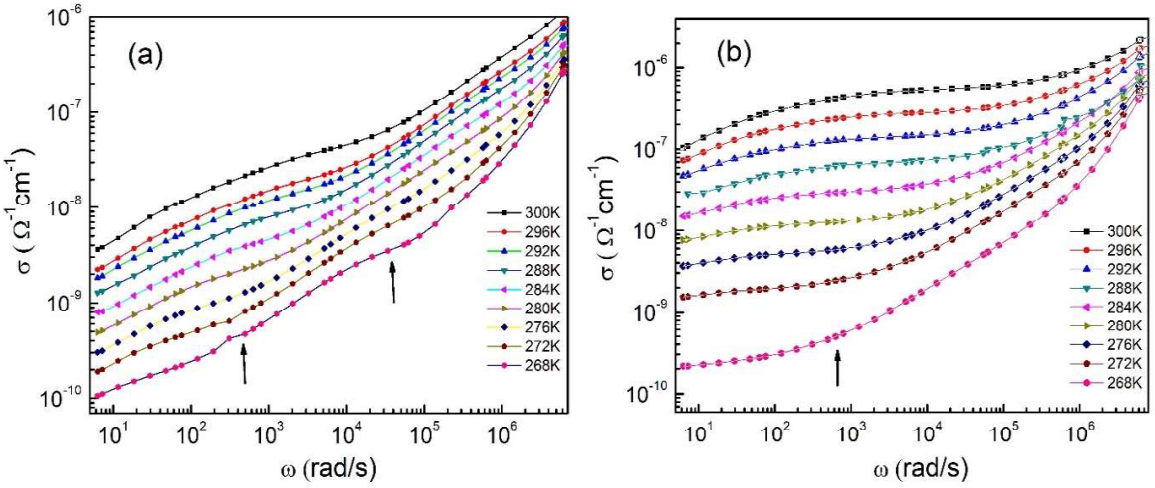

Figure 4.6 *Frequency dependent conductivity at different temperatures for (a) 0 NTP and (b) 40 NTP hybrid SPEs. The arrow indicates two well separated dc to dispersion regions, more apparently visible at lower temperatures.*

The onset of both the dc to dispersion regions (Fig. 4.6a and b) shift to higher frequencies as the temperature increases. This further suggests that for both processes, conductivity and structural relaxations are indeed temperature dependent. From the low frequency plateau

region, the dc (total) conductivity values were obtained and plotted as a function of temperature in Fig. 4.7.

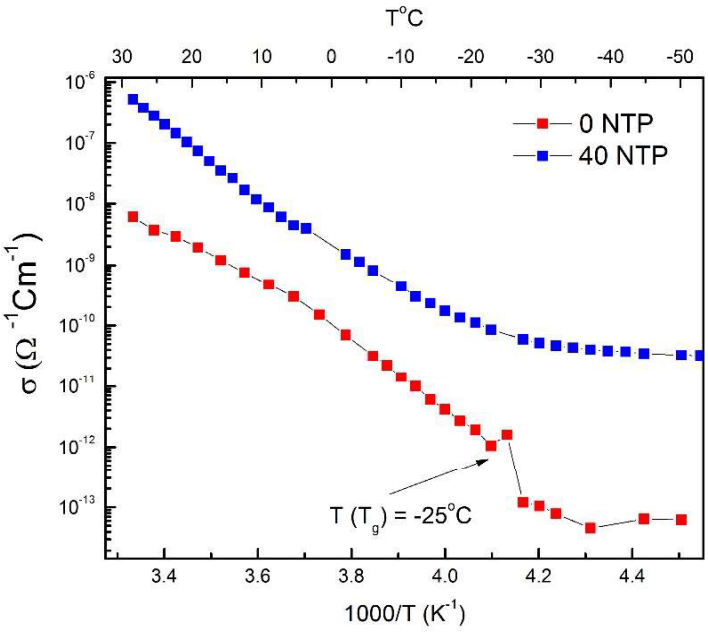

Figure 4.7 *Temperature dependent dc conductivity for the sample with 0 NTP and 40 NTP.*

Fig. 4.7 shows the temperature dependence of ionic conductivity (σ_{dc}) below ambient temperatures for 0 NTP and 40 NTP. 40 NTP exhibits higher conductivity than that of 0 NTP. It is evident that for 0 NTP (O/Li ratio of 31/1), the conductivity obeys Vogel-Fulcher-Tammann (VFT) viz. equation 1.

$$\sigma\,(T) = AT^{\frac{1}{2}}\left(-\frac{B}{K_B(T-T_o)}\right) \qquad (1)$$

where A is the pre-exponential factor, K_B is the Boltzmann's constant, T is the temperature in absolute scale, T_0 is the Vogel temperature and B is the pseudo activation energy. As described by various earlier workers [9], this non-linear behavior of the dc ionic conductivity corresponds to the ion transport through segmental relaxation of the host polymer which is apparently seen in - 30°C to -20°C temperature range. However, in this similar range of temperature, unlike 0 NTP, the 40 NTP composite exhibits apparent Arrhenius behavior. This readily suggests two separate mechanisms for samples with and without NTP. Arrhenius-like behavior of the dc conductivity suggests that the motion of the cations is hardly because of the structural relaxation of the polymer chains, but mostly through some other pathways.

As also noted in Fig. 4.7, the ionic conductivity for 0 NTP sample shows a notable drop at a temperature of ~ - 25°C. Such a drop may be due to the freezing of polymer segmental motion and hence freeze the ionic motion. However, different behavior is again noted for 40 NTP sample below -20°C. As apparent, the dc conductivity shows a saturation below freezing of polymer chains. It may be suggested that when the polymer is below T_g, the reinforced NTP in the matrix plays an important role and provides conduction pathways. The conductivity saturation may be attributed to poor thermally activated behavior in NTP.

Electric modulus (M″- ω) spectra have also been studied. It is known that M″ formalism suppresses the electrode polarization effect observed in the low frequency region and mainly provides information about electrical transport through bulk [9–12]. Fig. 4.8 (a) and (b) show the behavior of electric modulus (M″) with frequency for 0 NTP and 40 NTP at various temperatures. For comparison, the spectra were obtained at similar temperatures.

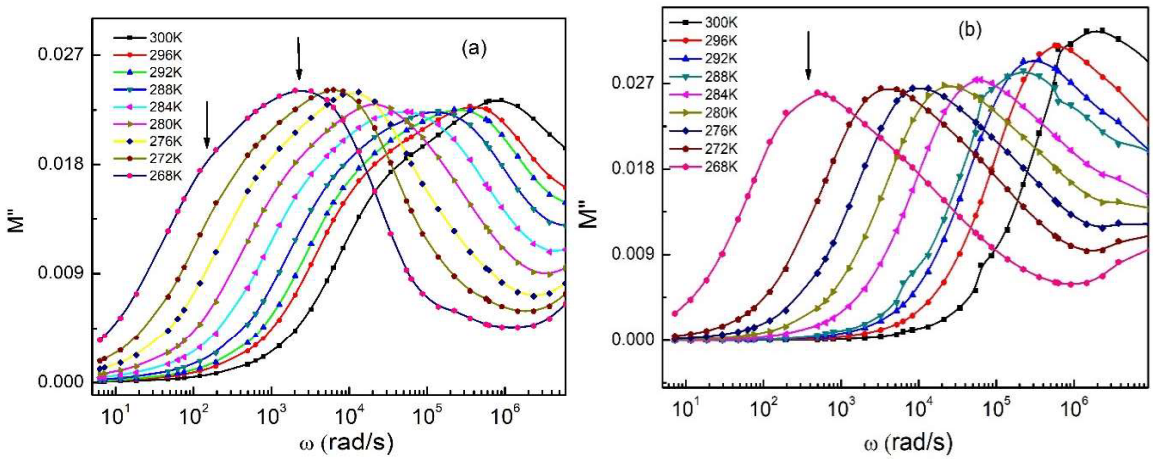

Figure 4.8 *Frequency dependence of electric modulus (M″) for 0 NTP and 40 NTP composites with temperature (for $T > T_g$).*

As described previously [12], pure PEO exhibits two apparent merged-up peaks in M″- ω spectra, attributed to long range ionic motion of impurity (at lower frequencies) and structural relaxation of polymer (at higher frequencies). In the present case, for 0 NTP, very similar behaviour is observed that suggests polymer chains are able to perform relaxation. In addition, long range ionic motion is also promoted in 0 NTP that may be through ion chain coupling. On the other hand, for 40 NTP, the second peak in M″- ω is not apparently visible, that may suggest suppression of chain relaxation due to reinforcement of NTP in the matrix. Therefore,

ion chain coupling though may exist, but not predominantly. The composite with NTP appears to support a dominant single process of ion migration. The M″- ω behavior for 40 NTP is in agreement with that of σ′- ω behavior where a single plateau is only observed, referring to a predominantly single mechanism of ionic transport.

Since the salt ion concentration in the compositions was kept constant to 10 wt%, NASICON crystallites must play a role in conductivity rise, particularly the pathways they may provide for ion transport through surface or bulk. Therefore, ionic mobility was measured using TIC technique (Discuss in Chapter 2) to get an insight into possible pathways for ionic transport. Transient ionic current behavior with time on reversal of polarity is shown for some compositions in Fig. 4.9. The ion mobility is reported for five compositions in Table 4.1.

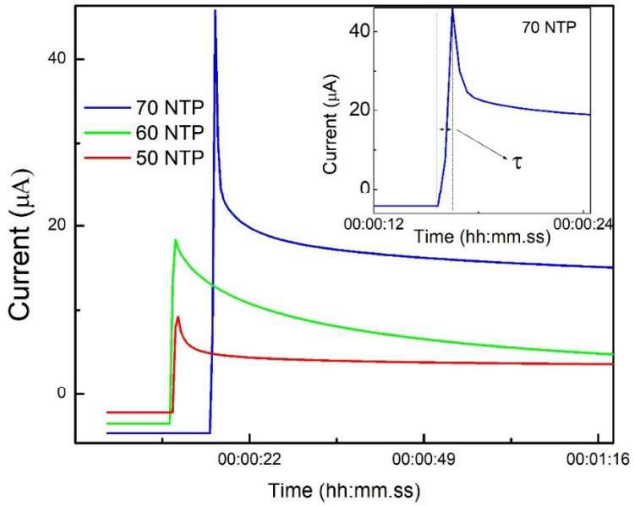

Figure 4.9. *Transient ionic current versus time for 50 NTP, 60 NTP and 70 NTP with polarization voltage of 0.5 V. Inset: Time of flight (τ) measurement from 70 NTP on an extended scale.*

Table 4.1 Ionic mobility using TIC technique for various compositions.

Sample	O/Na^+ ratio	μ (cm^2/V-s)
0 NTP	31/1	$9.2 (\pm 0.2) \times 10^{-3}$
40 NTP	18/1	$9.4 (\pm 0.2) \times 10^{-3}$
50 NTP	15/1	$9.1 (\pm 0.2) \times 10^{-2}$
60 NTP	12/1	$9.6 (\pm 0.2) \times 10^{-2}$
70 NTP	9/1	$9.9 (\pm 0.2) \times 10^{-2}$

The values obtained for polymer films without NASICON content are almost comparable to those reported in previous investigations [13]. As apparent, a significant rise in the mobility is observed for samples with high NTP content in the matrix, which suggests new pathways due to the presence of NTP in the polymer matrix. Alternatively, in presence of NTP grains, the ionic response to an external electric field improves which leads to fast ionic transport.

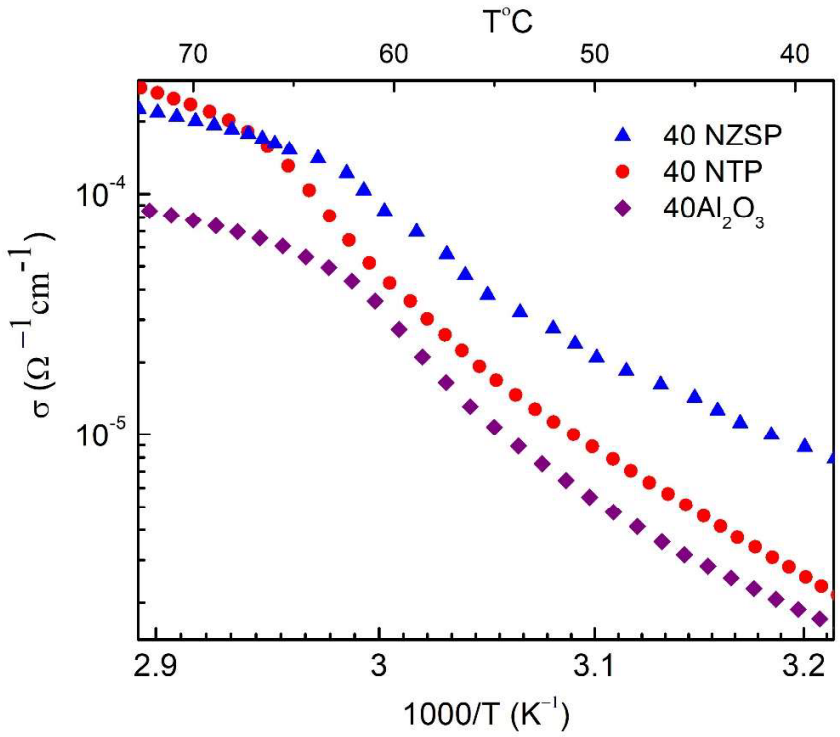

Figure 4.10 *Temperature dependence of dc conductivity for 10NaI-90(60PEO40 M), where M corresponds to dispersoids NTP, Al_2O_3 and NZSP ($Na_3Zr_2Si_2PO_{12}$) of almost same crystallite size of ~ 30 nm.*

Further, composites with different fillers (of the same size) were examined to understand the role of the electrical conductivity of NASICON in enhancing the overall ionic conductivity of the hybrid composites. As shown in Fig. 4.10, the conductivity of filler dictates the electrical transport. For insulting Al_2O_3, the conductivity is lowest, whereas, samples dispersed with the highest conducting NASICON i.e $Na_3Zr_2Si_2PO_{12}$ (NZSP) crystallites exhibit much superior conductivity. Therefore, repeatedly one observes that electrical conductivity of NTP (or any other NASICON analogue) plays a major role in order to tailor the overall conductivity of the

hybrid composite. Thus from here onwards, the discussion is around polymer matrix dispersed with the highest conducting NASICON viz. NZSP.

4.2 NaI-(PEO-NZSP) system

The samples under discussion are $10NaI\text{-}90[PEO_{1-x}NZSP_x]$ where $0 \leq x \leq 0.7$. The compoite with x = 0 here after abbreviated as 0 NZSP, and similarly for x = 0.1 as 10 NZSP and so on upto x = 0.7 as 70 NZSP. Importantly, samples for $x \leq 0.4$ were films and $x \geq 0.5$ were pellet.

4.2.1 X-ray diffraction and FESEM

The XRD patterns for these hybrid PEO-$Na_3Zr_2Si_2PO_{12}$ films are shown in Fig. 4.11a. The characteristic peaks corresponding to NZSP crystallites quite match well with the reported values [14]. The crystallite size for NZSP using Debye-Scherrer relation is found to be ~ 30 nm. The peaks corresponding to PEO and NZSP are apparent in the patterns of hybrid composites, viz. 40 and 70 NZSP (Fig. 4.11a).

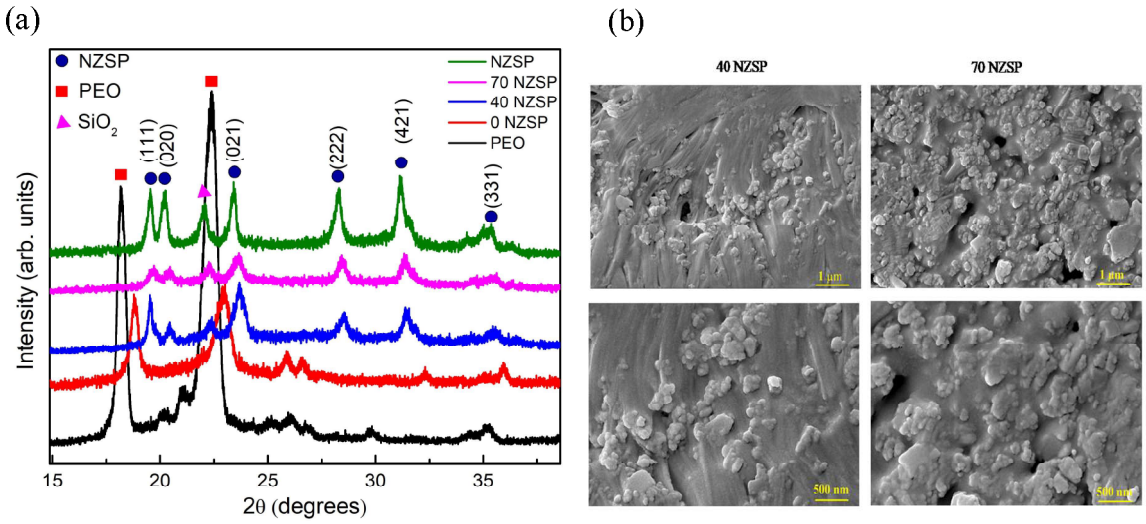

Fig. 4.11 *(a) XRD patterns for composites 10NaI-90[PEO1-xNZSP$_x$], where x = 0, 0.4, 0.7 along with pristine PEO and NZSP, indexing as per* [15] *(b) FESEM images for 40 and 70 NZSP composite at 1 μm and 500 nm scale*

Similar to previous observations, with increasing NZSP content, the polymer peaks significantly get suppressed and seen shifted as well. The significant change in the area under the peak and position of the PEO peak suggests its amorphization due to increasing NZSP

content in the matrix. Further, no new peak appears in the XRD spectra that readily suggests the existence of NZSP and polymer in separate phases.

Fig. 4.11b shows the surface morphology for 40 NZSP and 70 NZSP composites at 500nm and 1µm scale. As evident, in 40 NZSP sample, ceramic crystallites are in a relatively small amount and seen embedded between polymer layers though distribution appears less dense. The structure for composite 70 NZSP apparently suggests ceramic particles occupying a large volume fraction in the polymer matrix maintaining a dense and quite even distribution of grains. There is no agglomeration/segregation evident at least on the surface.

4.2.2 Electrical properties

Fig. 4.12 describes conductivity investigations on 10NaI_90[$PEO_{1-x}NZSP_x$] composites. The temperature-dependent ionic conductivity (1 kHz) with NZSP content is shown in Fig. 4.12a that exhibits apparent Arrhenius behavior.

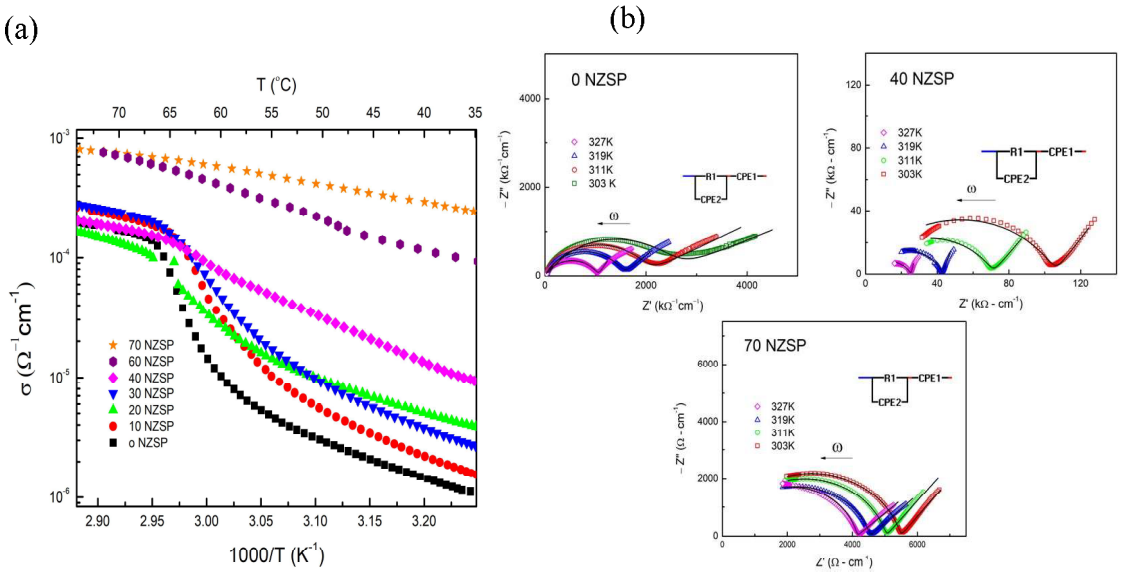

Fig. 4.12 *(a) Temperature dependence (1 kHz) of ionic conductivity for composites 10NaI-90[$PEO_{1-x}NZSP_x$], where $0 \leq x \leq 0.7$ and, (b) Nyquist plots (normalized with thickness for comparison and area of cross section is kept same for all samples) for 0, 40, and 70 NZSP at different temperatures for cell configuration of SS|SPE|SS. The solid line in the Nyquist plot shows the best fit using the equivalent circuit in the inset.*

Similar to earlier composites, for the lower content of NZSP in the polymer matrix ($x \leq 0.4$), the melting event (T_m) of the PEO is prominently observed. The same is gradually suppressed for samples with higher NZSP content. Crystallinity of PEO appears to be completely suppressed for larger content of NZSP which is consistent with other hybrid composites. As observed in Fig. 4.12a, the ionic conductivity monotonically increases with NZSP content, and for 70 NZSP, it reaches an appreciably high value of ~ 10^{-4} Ω^{-1}-cm^{-1} at room temperature.

Fig. 4.12b shows Nyquist plots for composites with x = 0, 0.4 and 0.7 at various temperatures. Evidently, the plots exhibit similar behavior for all compositions i.e. a semicircle at higher frequencies followed by a spike/spur at lower frequencies. The plots were further fitted using the combination of (R1||Q1)*Q2, (where R and Q represent resistive part and constant phase element, respectively). From the low-frequency intercept of the semicircle, the total resistance (R1) was thus obtained.

As seen, the resistance R decreases with NZSP content. As observed in Fig. 4.12a, 70 NZSP (i.e. with 63 wt % NZSP) exhibits a maximum ionic conductivity. In the further study, attention has been given to a composite with the highest NZSP content (63 wt%) and an effect of salt variation was investigated.

4.3 NZSP-(PEO-NaI) system

The samples (in the thick film form of thickness 450 μm) under discussion are 63NZSP-37($PEO_{1-x}NaI_x$) where x = 0.03, 0.07, 0.11 and 0.13.

4.3.1 Electrical properties

The electrical and structural properties of the composites 63NZSP-37($PEO_{1-x}NaI_x$) were studied. Nyquist plots and corresponding fitted spectrum using a combination of resistances (R) and constant phase elements (CPE) for composite with x = 0.03 (inset) and 0.13 are shown in Fig. 4.13a. As evident, the plots exhibit dissimilar nature for these low and high salt content samples. For composite with x = 0.03, a single depressed semicircle is observed followed by a spike at lower frequencies. No separate contribution of the phases can be estimated here, thus R1 is attributed to the total resistance of the composite. However, for a sample with x = 0.13, the semicircle appears to be shifted away from the origin. This readily suggests two different electrical transport mechanisms represented by respective models (inset).

Resistance R1, thus, can be attributed to bulk transport (R_b) whereas, R2 to a relatively poor conducting region, maybe the grain–grain interface, where polymer's presence is likely. Thus, R2 may again be assigned to polymer-grain boundary interfacial properties (R_{PGB}). The exact determination of conductivities of different phases (corresponding to R_b and R_{PGB}) and their temperature dependence is rather tricky due to limited frequency range. However, safely the total conductivity is obtained from low frequency intercept with the inclined line.

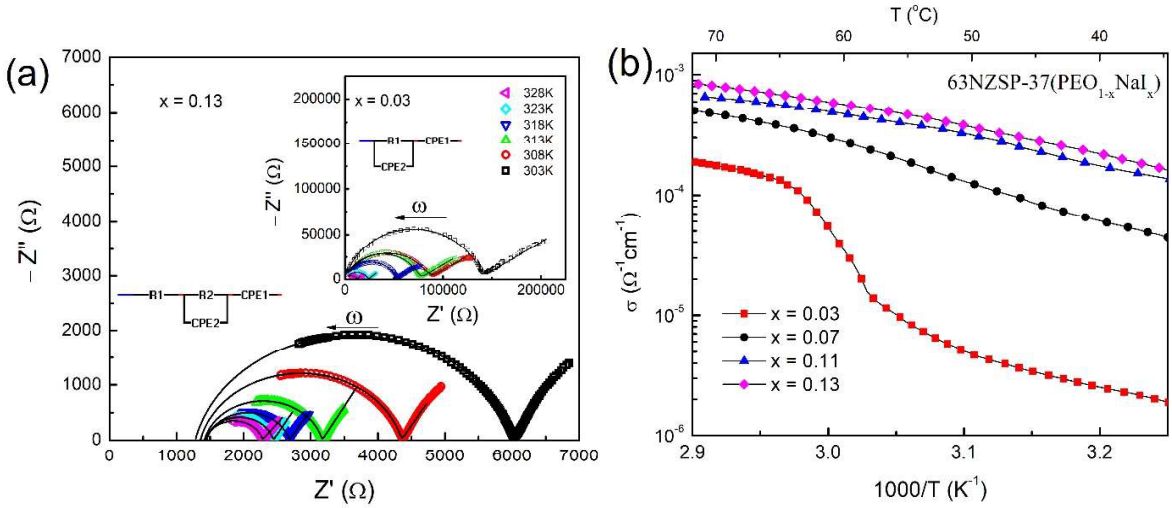

Figure 4.13 *(a) Nyquist plots for composites with x = 0.13 and 0.03 (inset). Dotted lines represent corresponding fitted models. (b) Temperature dependence of total conductivity obtained from Nyquist plots for all composites. Inset: σ-T cycles (1 kHz) at a heating rate of 1°C min^{-1} to observe effect of polymer melting on electrical transport.*

Fig. 4.13b shows the temperature dependence of total conductivity obtained from Nyquist plots. Apparently, for higher salt content the conductivity almost increases linearly with temperature. It exhibits a high value of $10^{-4}\ \Omega^{-1}\ cm^{-1}$ at room temperature for x = 0.13, comparable to bulk conductivity of NZSP [14]. The activation energy for the highest conducting composition (0.33 eV) is also found to be comparable to NASICONs reported earlier [14]. Such a rise must be attributed to a significant alteration of conductivity at grain-grain interface. The interface, where Na^+ ion rich polymer is incorporated, possibly facilitates smooth inter-grain transport. On heating at a controlled rate (Fig. 4.13b inset), conductivity shows a rapid increase near polymer melting temperature for x = 0.03. For x = 0.07–0.11, polymer is largely substituted by the salt, therefore PEO melting (T_m) event is not evident in

the σ-T behavior. This may also be due to a significant change in the O/Na ratio from 30:1 (for x = 0.03) to 6:1 (x = 0.13) that leads to a decrease in PEO crystallinity. Thus composites with x = 0.07–0.13 exhibit reproducible Arrhenius behavior of σ-T cycles at least up to 100 °C.

4.3.2 X-ray diffraction and FESEM

Fig. 4.14 shows XRD patterns for $Na_3Zr_2Si_2PO_{12}$ [16][17][15] and hybrids. No precipitation is evident even for high salt content samples. Since salt is in the dissolved state, a large mobile ion concentration is therefore expected in the polymer existing at inter-grain voids and grain boundaries.

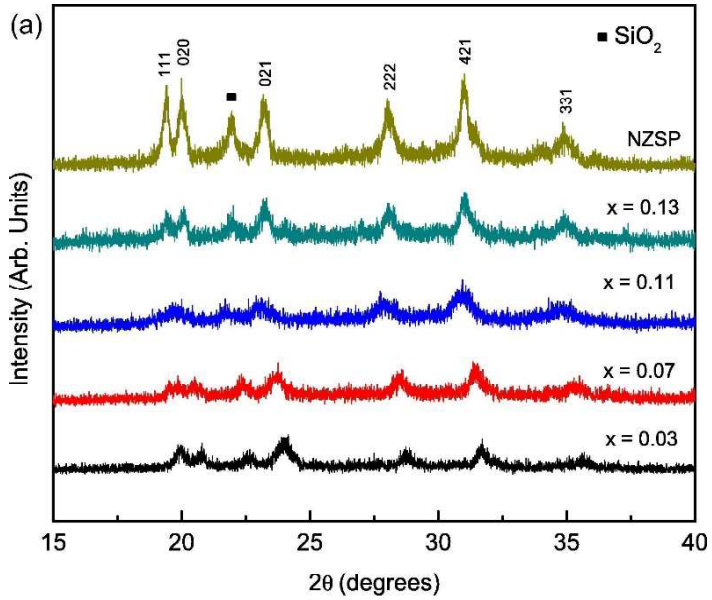

Figure 4.14*. XRD patterns for composites with x = 0.03–0.13. Indexing as per* [15]

FESEM images of composites with x = 0.03 and 0.13 are shown in Fig. 15 a and b. As apparent for lower salt content, polymer is apparently seen surrounding the nano-grains of NZSP. For large salt content when the polymer is in small amount, grains are more closely packed. In both cases, composites appear homogeneous.

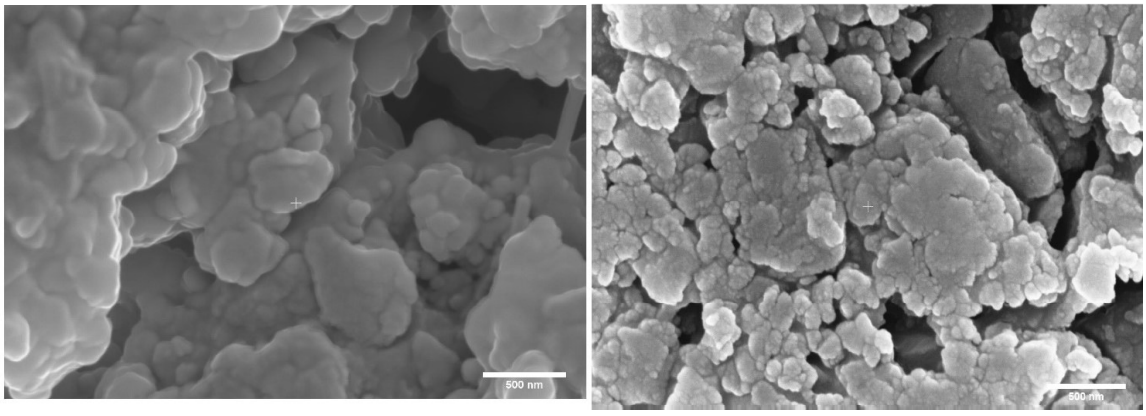

(a) (b)

Figure 4.15 *(a) and (b) FESEM images for composite with x = 0.03 and 0.13, respectively.*

4.4. Summary

(i) (i) Na^+ ion based NTP as well as NZSP dispersed polymer composites could be prepared in a wide range of the composition. Similar to Li^+ ion dispersed systems, these samples were found to be embedded with evenly distributed active crystallite fillers of uniform size.

(ii) The addition of NTP/NZSP suppresses the crystallization of PEO. For large filler content, thermal cycling stability notably improves. This is consistent with those of Li^+ ion systems.

(iii) Results again suggest that the quality of grain interior conductivity plays a major role in achieving high conductivity in these composites.

(iv) The addition of NASICON seems to be affecting the mechanism of transport and also the ion mobility, particularly for large content of fillers.

(v) Composite with 63 wt% NSZP with x = 0.13 NaI concentration exhibits a maximum ionic conductivity ~ 10^{-4} Ω^{-1} cm^{-1}. This is one of the highest conductivity reported so far in Na^+ ion solid electrolytes.

(vi) These results along with those on Li^+ ion systems (chapter 3) strongly suggest that NASICON crystallites not only facilitate electrical transport by creating amorphous regions, but also enhance conductivity by providing pathways, either through their bulk or through states existing at polymer-NTP interface. For this, however, it is required to

show some evidence of decoupling of cations from the polymer matrix. This will be presented in the next chapter.

Reference:

[1] Y. Wang, K.S. Chen, J. Mishler, S.C. Cho, X.C. Adroher, A review of polymer electrolyte membrane fuel cells: Technology, applications, and needs on fundamental research, Appl. Energy. 88 (2011) 981–1007. https://doi.org/10.1016/j.apenergy.2010.09.030.

[2] M.E. Abdelhamid, A.P. O'Mullane, G.A. Snook, Storing energy in plastics: A review on conducting polymers & their role in electrochemical energy storage, RSC Adv. 5 (2015) 11611–11626. https://doi.org/10.1039/c4ra15947k.

[3] L. Long, S. Wang, M. Xiao, Y. Meng, Polymer electrolytes for lithium polymer batteries, J. Mater. Chem. A. 4 (2016) 10038–10069. https://doi.org/10.1039/C6TA02621D.

[4] A. Ponrouch, D. Monti, A. Boschin, B. Steen, P. Johansson, M.R. Palacín, Non-aqueous electrolytes for sodium-ion batteries, J. Mater. Chem. A. 3 (2015) 22–42. https://doi.org/10.1039/C4TA04428B.

[5] A. Boschin, P. Johansson, Characterization of NaX (X: TFSI, FSI) - PEO based solid polymer electrolytes for sodium batteries, Electrochim. Acta. 175 (2015) 124–133. https://doi.org/10.1016/j.electacta.2015.03.228.

[6] C. Vaalma, D. Buchholz, M. Weil, S. Passerini, A cost and resource analysis of sodium-ion batteries, Nat. Rev. Mater. 3 (2018) 18013. https://doi.org/10.1038/natrevmats.2018.13.

[7] X. Yang, K. Wang, X. Wang, G. Chang, S. Sun, Carbon-coated NaTi2(PO4)3 composite: A promising anode material for sodium-ion batteries with superior Na-storage performance, Solid State Ionics. 314 (2018) 61–65. https://doi.org/10.1016/j.ssi.2017.11.016.

[8] D.P. Almond, C.C. Hunter, A.R. West, The extraction of ionic conductivities and hopping rates from a.c. conductivity data, J. Mater. Sci. 19 (1984) 3236–3248. https://doi.org/10.1007/BF00549810.

[9] S.B. Aziz, T.J. Woo, M.F.Z. Kadir, H.M. Ahmed, A conceptual review on polymer electrolytes and ion transport models, J. Sci. Adv. Mater. Devices. 3 (2018) 1–17.

https://doi.org/10.1016/j.jsamd.2018.01.002.

[10] G. Mao, R.F. Perea, W.S. Howells, D.L. Price, M.-L. Saboungi, Relaxation in polymer electrolytes on the nanosecond timescale, Nature. 405 (2000) 163–165. https://doi.org/10.1038/35012032.

[11] S. Das, A. Ghosh, Charge Carrier Relaxation in Different Plasticized PEO/PVDF-HFP Blend Solid Polymer Electrolytes, J. Phys. Chem. B. 121 (2017) 5422–5432. https://doi.org/10.1021/acs.jpcb.7b02277.

[12] B.K. Money, K. Hariharan, J. Swenson, B. K. Money, K. Hariharan, J. Swenson, B.K. Money, K. Hariharan, J. Swenson, B. K. Money, K. Hariharan, J. Swenson, Relation between structural and conductivity relaxation in PEO and PEO based electrolytes, Solid State Ionics. 262 (2014) 785–789. https://doi.org/10.1016/j.ssi.2013.09.033.

[13] A. Chandra, A. Chandra, K. Thakur, Na^+ Ion Conducting Hot-pressed Nano Composite Polymer Electrolytes, Port. Electrochim. Acta. 30 (2012) 81–88. https://doi.org/10.4152/pea.201202081.

[14] H. Park, M. Kang, Y.C. Park, K. Jung, B. Kang, Improving ionic conductivity of Nasicon (Na3Zr2Si2PO12) at intermediate temperatures by modifying phase transition behavior, J. Power Sources. 399 (2018) 329–336. https://doi.org/10.1016/j.jpowsour.2018.07.113.

[15] D. Chen, F. Luo, W. Zhou, D. Zhu, Dielectric properties in the microwave range of Na3Zr2Si2PO12 ceramics, Mater. Lett. 221 (2018) 172–174. https://doi.org/10.1016/j.matlet.2018.03.128.

[16] A.G. Jolley, G. Cohn, G.T. Hitz, E.D. Wachsman, Improving the ionic conductivity of NASICON through aliovalent cation substitution of Na3Zr2Si2PO12, Ionics (Kiel). 21 (2015) 3031–3038. https://doi.org/10.1007/s11581-015-1498-8.

[17] M. Samiee, B. Radhakrishnan, Z. Rice, Z. Deng, Y.S. Meng, S.P. Ong, J. Luo, Divalent-doped Na3Zr2Si2PO12 natrium superionic conductor: Improving the ionic conductivity via simultaneously optimizing the phase and chemistry of the primary and secondary phases, J. Power Sources. 347 (2017) 229–237. https://doi.org/10.1016/j.jpowsour.2017.02.042.